



TITLE:

Performance validation of sodium-ion batteries using an ionic liquid electrolyte

AUTHOR(S):

Fukunaga, Atsushi; Nohira, Toshiyuki; Hagiwara, Rika; Numata, Koma; Itani, Eiko; Sakai, Shoichiro; Nitta, Koji

CITATION:

Fukunaga, Atsushi ...[et al]. Performance validation of sodium-ion batteries using an ionic liquid electrolyte. Journal of Applied Electrochemistry 2016, 46(4): 487-496

ISSUE DATE:

2016-04

URL:

<http://hdl.handle.net/2433/230385>

RIGHT:

This is a post-peer-review, pre-copyedit version of an article published in 'Journal of Applied Electrochemistry'. The final authenticated version is available online at: <https://doi.org/10.1007/s10800-016-0940-6>; The full-text file will be made open to the public on 1 April 2017 in accordance with publisher's 'Terms and Conditions for Self-Archiving'; This is not the published version. Please cite only the published version.; この論文は出版社版ではありません。引用の際には出版社版をご確認ください。

Performance validation of sodium-ion batteries using an ionic liquid electrolyte

Atsushi Fukunaga^{a,b}, Toshiyuki Nohira^{c,*}, Rika Hagiwara^{a,*}, Koma Numata^b, Eiko Itani^b, Shoichiro Sakai^b, Koji Nitta^b

a. Graduate School of Energy Science, Kyoto University, Yoshida-honmachi, Sakyo-ku, Kyoto 606-8501, Japan.

b. Sumitomo Electric Industries Ltd., 1-1-3 Shimaya, Konohana-ku, Osaka 554-0024, Japan.

c. Institute of Advanced Energy, Kyoto University, Gokasho, Uji, Kyoto 611-0011, Japan.

*Corresponding authors: Tel.: +81-774-38-3500; Fax: +81-774-38-3499 (T. Nohira), Tel.: +81-75-753-5822; Fax: +81-75-753-5906 (R. Hagiwara). E-mail addresses: nohira.toshiyuki.8r@kyoto-u.ac.jp, hagiwara@energy.kyoto-u.ac.jp.

Abstract

Charge–discharge properties of sodium–ion batteries using the Na[FSA]–[C₃C₁pyrr][FSA] (FSA: bis(fluorosulfonyl)amide, C₃C₁pyrr: *N*–methyl–*N*–propylpyrrolidinium) ionic liquid were investigated over a temperature range of 273–363 K. NaCrO₂ and hard carbon (HC) were used as positive electrode and negative electrode active materials, respectively, and their fundamental charge–discharge characteristics were examined with coin–type half–cells. A 1.5 mAh coin–type full cell composed of HC/NaCrO₂ showed excellent cycle properties, maintaining 90% of its initial capacity after 1000 cycles at 333 and 363 K. The 1.5 mAh full cell also exhibited a high charge–discharge energy efficiency of 97.5% at 363 K and C/5 rate. A large–sized prismatic HC/NaCrO₂ full cell with a capacity of 27 Ah was fabricated by a mass production process, and its performance was confirmed to be comparable with that of the 1.5 mAh coin–type cell.

Key words: sodium secondary battery; ionic liquid; bis(fluorosulfonyl)amide; NaCrO₂ positive electrode; hard carbon negative electrode; full cell performance

1. Introduction

The demand for secondary batteries for energy-storage devices has recently experienced significant growth for use in important applications such as load leveling, emergency power supply devices, and smart grids [1-2]. As high-performance secondary batteries, lithium-ion batteries (LIBs) are popular not only for mobile applications but also for electric vehicle and household uses [3-4]. However, difficulties in locating and extracting material resources for LIBs are anticipated in the near future, because such devices employ minor metals like cobalt and nickel [5-15]. Even for lithium, a stable supply seems to be problematic over the long term because high-quality lithium resources are unevenly distributed in the earth's crust, occurring mainly in China and South America [16-18]. Thus, the research and development of secondary batteries using only easily available raw materials such as sodium has become an active field of investigation. In support of this fact, the number of reports on sodium secondary batteries has risen rapidly in the past 2-3 years [5-15]. Sodium, which can be easily obtained from seawater or the earth's crust, possesses a reasonably negative standard redox potential of -2.714 V vs. the standard hydrogen electrode (SHE). Furthermore, many advanced technologies designed for use in LIBs are expected to be applicable in sodium secondary batteries [5-15].

The development of sodium secondary batteries has a long history. Batteries using β -alumina electrolyte have been studied for many years [19-24], and Na/S and Na/NiCl₂ batteries are currently in practical use as large-scale energy-storage devices for mega solar power plants and wind farms. However, these batteries have less-than-ideal operating conditions for such industrial applications. The β -alumina electrolyte needs an operating temperature of approximately 573 K to raise its conductivity. Furthermore, Na/S and Na/NiCl₂ batteries require liquid sodium metal, which is an extremely hazardous material. Thus, storage and installation of Na/S and Na/NiCl₂ batteries are restricted because of their large size and the regulations placed on the use of sodium metal.

At the same time, reports on sodium secondary batteries using organic electrolytes have recently increased [25-27]. These reports highlight promising advantages of these batteries, such as energy density, cost, and material abundance. However, the use of organic solvents in batteries, similar to conventional LIBs, requires safety considerations, because an accident involving such batteries can be destructive (and potentially lethal) for large-scale batteries. Moreover, the required organic solvents cannot be used at intermediate or high temperatures because of their high volatility and the low stability

of solid–electrolyte interphases (SEIs) on negative electrodes. Accordingly, large–scale and assembled sodium secondary batteries using organic solvents must be equipped with cooling systems, similar to LIBs, in order to be used safely.

The development of safe and high–performance electrolytes is badly needed in order to address the drawbacks listed in the previous paragraph. We have developed several ionic liquids for sodium secondary battery electrolytes that have high thermal stabilities, high ionic conductivities, and wide electrochemical windows [28–31]. We have demonstrated their actual operation using Na/Na[TFSA]–Cs[TFSA]/NaCrO₂ (TFSA: bis(trifluoromethylsulfonyl)amide; operating temperature: 423 K) [32], Na/Na[FSA]–K[FSA]/NaCrO₂ (FSA: bis(fluorosulfonyl)amide; operating temperature: 353 K) [33], and Na/Na[FSA]–[C₃C₁pyrr][FSA]/NaCrO₂ (C₃C₁pyrr: *N*–methyl–*N*–propylpyrrolidinium, operating temperature: 253–353 K) [34]. We have also confirmed excellent cycle performances, rate capabilities, and wide operating temperatures for batteries using these ionic liquids as the electrolyte medium and a NaCrO₂ positive electrode. Recently, Xia et al. reported the stabilities of deintercalated Na_{0.5}CrO₂ (fully charged state) in nonaqueous solvents [35]. Xia reported that NaCrO₂ is the best active material for the operation of sodium secondary batteries over a wide temperature range.

In previous studies, however, sodium metal was used as a negative electrode. Although dendrite deposition of sodium metal is suppressed by operating at a temperature close to the melting point of sodium (371 K) [34], it is difficult to completely prevent dendrite deposition, especially at lower operating temperatures. Referring to the reports on hard carbon (HC) by Komaba et al. [36–38], we also investigated HC negative electrodes [39] to avoid the use of sodium metal negative electrodes. Unfortunately, when the Na[FSA]–K[FSA] ionic liquid was used, HC irreversibly reacted with K⁺ cations during the charge–discharge test. However, good reversibility and rate capability were obtained by using the Na[FSA]–[C₃C₁pyrr][FSA] ionic liquid [39].

Much research has been conducted on sodium secondary batteries using half–cells, especially coin–type half–cells. Some of the work using half–cells reported the results of long–term cycle life of batteries. However, investigations on long–term cycle life should also be verified by using full cells. Unfortunately, few studies have been conducted using “full cells.” Although full cell performance is predictable from the results of positive and negative electrode half–cell tests, actual verification using full cells is imperative for the practical applications of sodium secondary batteries. Ideally, the verification

should also include the scaling up of full cells, because the most expected application of such cells is in large-size batteries. In this study, we first investigate the fundamental charge-discharge characteristics of NaCrO₂ positive electrodes and HC negative electrodes using Na[FSA]–[C₃C₁pyrr][FSA] ionic liquids and coin-type half-cells at 333 and 363 K. Furthermore, we examine, for the first time, the detailed full cell performance, including the long-term cycle life of a 1.5 mAh HC/NaCrO₂ cell using a coin-type cell over the temperature range of 273–363 K. Finally, we fabricate a large-sized prismatic full cell with a capacity of 27 Ah and compare the performance with that of a coin-type cell.

2. Experimental

Na[FSA] (Mitsubishi Materials Electronic Chemicals Co., Ltd., Japan, >99.0%) and [C₃C₁pyrr][FSA] (Kanto Chemical Co., Inc. Japan, >99.0%) were dried under vacuum at 333 K for 24 h. The Na[FSA]–[C₃C₁pyrr][FSA] ionic liquid (Na[FSA]:[C₃C₁pyrr][FSA] = 20:80 mol%) was prepared by mixing the salts under magnetic stirring. Inductively coupled plasma atomic emission spectroscopy (ICP–AES) and ion chromatography analysis showed that impurities in the electrolytes, such as metallic cations or halide anions, were less than 10 ppm. The electrochemical windows for Na[FSA]–[C₃C₁pyrr][FSA] systems have been previously measured to be 5.2 V at 353 K [34]. The water content of the electrolyte was determined to be less than 10 ppm by the Karl Fischer titration method.

The positive electrode active material, NaCrO₂, was prepared using a solid phase method. Equimolar amounts of Na₂CO₃ and Cr₂O₃ were mixed and then baked at 1123 K for 7 h under Ar flow. Figure 1 shows an XRD pattern of the obtained sample, confirming that the sample is NaCrO₂ with no impurity. NaCrO₂ thus prepared was well mixed with acetylene black (Denka Black, purity >99.99%) and PVdF (Kureha) in *N*-methyl-2-pyrrolidone (Kishida Chemical Co., Ltd., >99.5%) at a weight ratio of 85/10/5 using a dispersion mixer. The obtained slurry was then coated onto an aluminum foil current collector and pressed by a roller press. The loading weight was 13.5 (mg–NaCrO₂) cm^{–2} (ca. 1.7 mAh in theoretical capacity 125 mAh (g–NaCrO₂)^{–1}). The negative electrode active material, HC, was used as purchased (CARBOTRON P, Kureha Battery Materials Japan Co., Ltd.). HC and the polyamide-imide binder were mixed in *N*-methyl-2-pyrrolidone (Kishida Chemical Co., Ltd., >99.5%) at a weight ratio of 96/4 using a dispersion mixer. The obtained slurry was coated onto a current collector and pressed by a roller press. The loading weight was 5.2 (mg–HC) cm^{–2}.

Charge–discharge properties of Na/NaCrO₂ and Na/HC half–cells, and HC/NaCrO₂ full cell were measured with a 2032–type coin cell. A sodium foil (Aldrich, >99.9%) was used as the negative electrode for Na/NaCrO₂ and Na/HC half–cells. A microporous membrane (NPS050, Nippon Sheet Glass Co., Ltd., thickness: 50 μm) was used as the separator. Charge–discharge tests were conducted at a constant current rate by a computer–controlled charge–discharge unit (ABE 1024–05R1, Electrofield Corp). Current rate and cut–off voltages are shown in Table 1. Temperature of the cell was maintained at 273–363 K by a thermostatic oven during the charge–discharge tests.

In addition to a coin–type full cell, a 27 Ah prismatic HC/NaCrO₂ full cell was fabricated using a mass production process. Figure 2 shows the appearance of the fabricated 27 Ah cell. Positive electrodes, negative electrodes, and separators were the same as those used in the coin–type cell. Positive and negative electrode active materials were coated on both sides of the Al foil current collector. A bundle of electrodes and separators electrically connected in parallel via lead tabs. Na[FSA]–[C₃C₁pyrr][FSA] electrolyte was filled into an aluminum case (external size: 113 × 150 × 38 mm) and the lid sealed by laser welding. Charge–discharge tests of a 27 Ah HC/NaCrO₂ prismatic cell were conducted at a constant current rate in a thermostatic oven conducted by a computer–controlled charge–discharge unit (ABE 1028–5V, Electrofield Corp).

3. Results and discussion

3.1. NaCrO₂ half–cell (coin–type cell)

A typical charge–discharge curve of a coin–type Na/NaCrO₂ half–cell at 363 K is shown in Figure 3 (a). The shape of charge–discharge curve is derived from phase transition of Na_{1–x}CrO₂ ($x < 0.5$) during charge–discharge [6,43]. In our previous study, phase transitions of NaCrO₂ at 363 K were evaluated by ex–situ XRD measurements [43]. The desodiation of NaCrO₂ during charging produces following phase transition: rhombohedral O3 ($x < 0.03$) → monoclinic O'3 ($x = 0.2$) → monoclinic P'3 ($x > 0.34$). The notations of the phase were designed by Delmas [44]. The potential plateau around 2.9 V indicates the mixed phase of O3/O'3 or O'3/P'3, whereas the potential slope from 3.0 V to 3.3 V means the change of interslab distance of CrO₂ layers in single phase. The observed reversible capacity is 110 mAh g^{–1}, and the coulombic efficiency is >99.9%, which are almost the same numbers as those reported in our previous study [34]. Figures 3 (b) and (c) show discharge curves at 363 and 333 K, respectively, at

rates of 10–600 mA (g–NaCrO₂)^{–1}. The rate dependence of discharge capacity is also shown in Figure 4. It is seen that the Na/NaCrO₂ cell maintains almost the same discharge capacity of 110 mAh g^{–1} at discharge rates below 100 mA g^{–1} at both 333 and 363 K. In the case of 363 K, the discharge capacity gradually decreases with the discharge rate, but retains approximately 80 mAh g^{–1} even at 400 mA g^{–1}. In contrast, the discharge capacity markedly decreases at 333 K as the discharge rate increases over 200 mA g^{–1}. Specifically, in the discharge curves at 333 K, the voltage of the plateaus drop and its length shortens at values higher than 200 mA g^{–1}. These results indicate that the operating temperature has a significant effect on the discharge rate performance. These results suggest that Na⁺ ion insertion into the CrO₂ layer of NaCrO₂ is decelerated at lower temperatures.

3.2. Hard carbon half-cell (coin-type cell)

A typical charge–discharge curve for a Na/HC cell at 50 mA g^{–1} at 363 K is shown in Figure 5 (a). The observed reversible capacity is ca. 270 mAh g^{–1} and the coulombic efficiency is higher than 99%. The cycle properties of the Na/HC cell have already been reported in our previous study [39]. Discharge curves at various discharge rates of 25–1000 mA g^{–1} at 363 and 333 K are shown in Figures 5 (b) and (c), respectively. The outline shapes of discharge curves do not change even at 750 mA g^{–1} at 333 K and 1000 mA g^{–1} at 363 K. The observed positive shifts of the curves at higher discharge rates (> 250 mA g^{–1}) are likely due to IR drops, because the value of positive shift is proportional to the increment of discharge rate (current density).

Figure 6 shows the rate dependence of the discharge capacity at 333 and 363 K. The observed discharge capacities at the same discharge rate are almost identical at both temperatures, indicating that the rate of Na⁺ extraction from HC is not largely affected by temperature under the present experimental conditions. In summary, the HC negative electrode has excellent rate capability in the Na[FSA]–[C₃C₁pyrr][FSA] ionic liquid at 333 and 363 K. A comparison of Figure 4 with Figure 6 clearly indicates that the HC negative electrode has a superior rate capability than the NaCrO₂ positive electrode, in the present tests.

3.3. 1.5 mAh HC/NaCrO₂ full cell (coin-type cell)

Figure 7 (a) shows the charge–discharge curve for a 1.5 mAh HC/NaCrO₂ full cell operating in

the voltage range of 1.5–3.4 V at 0.3 mA and 363 K. The voltage plateaus observed at around 2.9 V on both the charge and discharge curves are derived from the character of the NaCrO_2 positive electrode. The monotonic voltage changes in the region of 1.5–2.7 V arise from the features of the HC negative electrode. The average discharge voltage is ca. 2.6 V. The observed cell capacity is 1.53 mAh, which corresponds to $102 \text{ mAh (g-NaCrO}_2\text{)}^{-1}$ for the positive electrode and $252 \text{ mAh (g-HC)}^{-1}$ for the negative electrode. Since the reversible capacities observed in the half-cell tests are $110 \text{ mAh (g-NaCrO}_2\text{)}^{-1}$ and $270 \text{ mAh (g-HC)}^{-1}$, the capacity utilizing ratios are calculated as ca. 93% for the NaCrO_2 and HC electrodes. Discharge curves at discharge rates of 0.3–9.0 mA (approximately 5/C–6C rate) at 363 and 333 K are shown in Figures 7 (b) and (c), respectively. Appreciable changes are observed from 9.0 mA at 363 K and 3.0 mA at 333 K. The observed charge–discharge characteristics are consistent with the results of the half-cells. A superior rate capability is achieved when the cell is operated at 363 K.

To check whether the HC/ NaCrO_2 full cell works at temperatures lower than 333 K, charge–discharge tests were conducted at 313, 298, 283, and 273 K. Figure 8 shows typical discharge curves at 0.3 mA and 298 K, and 0.15 mA at 283 K. The discharge capacities are 1.50 mAh at 298 K and 1.35 mAh at 283 K. This result confirms that the HC/ NaCrO_2 full cell is operable at room temperature or even lower than room temperature with moderate discharge rates. Figure 9 shows the rate dependence of the discharge capacity at 273–363 K. The designated capacity of 1.5 mAh is exerted at temperatures higher than 298 K. The rate capability steadily increases as the temperature increases. The highest rate capability is attained at 363 K.

Figure 10 shows the cycle properties of the 1.5 mAh HC/ NaCrO_2 full cell at 1.5 mA (1C) rate at 333 K and 363 K. Even for the fully charging and discharging tests, remarkably stable cycleability is obtained. The capacity is maintained up to 90% of the initial capacity after 1000 cycles. There is almost no difference in the capacity retentions between 333 K and 363 K. This stable cycleability at 363 K is an outstanding achievement, considering that conventional LIBs employing organic solvent–based electrolytes cannot be operated at such high temperatures. The long-term cycle stability in the intermediate temperature range is attributed to the high thermal stability of SEI films on HC negative electrodes as well as good thermal stability of the $\text{Na[FSA]}-\text{[C}_3\text{C}_1\text{pyrr]FSA}$ ionic liquid itself. Table 2 summarizes the coulombic and energy efficiencies for the HC/ NaCrO_2 full cell at a rate of 0.3 mA at 298, 333, and 363 K. The obtained coulombic efficiencies are higher than 99.7% for all temperatures.

Considerably high charge–discharge energy efficiencies are achieved: 96.9% at 333 K and 97.5% at 363 K. These values are comparable with, or better, than those of conventional LIBs at ambient temperature [40–41]. The slight decrease in the energy efficiency at 298 K (93.2%) is caused by the increase in the internal resistance due to lower ionic conductivity.

3.4 27 Ah HC/NaCrO₂ full cells (large–sized prismatic cell)

Based on the results for coin–type cells, large–size prismatic cells having a designed capacity of 27 Ah were fabricated. The weight and volume of the 27 Ah cell were 1.08 kg, and 0.644 L, respectively.

Figure 11 shows the charge–discharge curves for the 27 Ah HC/NaCrO₂ full cell at 298 and 333 K. The observed discharge capacity at a rate of 2.7 A is 27.3 Ah at 298 K, which is equal to the designed capacity. At 333 K, almost the same charge–discharge behavior is obtained, even at the higher rate of 10 A. The calculated volumetric and gravimetric energy densities of the 27 Ah cell are ca. 125 Wh L^{−1} and 75 Wh kg^{−1}, respectively. These values are comparable with those for large–scale prismatic LIBs in the early 2000s [42]. It should be noted that the shape of the charge–discharge curve for the 27 Ah cell is almost identical to that of a 1.5 mAh coin–type cell. Thus, it is expected that the performance of a large–sized full cell is well predicted by that of a coin–type cell. Actually, the calculated energy efficiencies at a rate of 5.4 A are 93.9% at 298 K and 96.8% at 333 K. These values are almost the same as those for coin–type cells shown in Table 2.

Figure 12 shows the rate dependence of discharge capacity for the 27 Ah full cell at 283, 298, 313, 333, and 363 K. Again, the rate capability is comparable with that for the 1.5 mAh coin–type cell. An especially superior rate capability is obtained at 333 and 363 K. On the other hand, the performance is unsatisfactory at 283 K, which is due to the lower conductivity of the ionic liquid. Figure 13 shows the cycleability of the 27 Ah full cell at a rate of 10 A at 333 K. This is also the fully charging and discharging test done in the same manner as the coin–type cell. The capacity retention after 500 cycles is 87%. Although this value is slightly lower than that of the 1.5 mAh coin–type cell shown in Figure 10, it is the same value as that of large–scaled prismatic LIBs used in the early 2000s [42]. Considering that the 27 Ah cell has been produced by an industrial process similar to that for conventional LIBs, it is safe to say that a large–sized HC/Na[FSA]–[C₃C₁pyrr][FSA]/NaCrO₂ cell can show further improvements in energy

density, power density (rate capability), energy efficiency, and cycleability with improved manufacturing technology.

As described in this section, HC/Na[FSA]–[C₃C₁pyrr][FSA]/NaCrO₂ cells exhibit high performance and long cycle life over a wide temperature range including a high temperature of 363 K. Thus, these cells are best expected to be used in new fields where conventional LIBs cannot be used. For example, near heated devices such as engines in hybrid electric vehicles (HEVs), or fuel cells in fuel cell vehicles (FCVs). This is highly beneficial even for electric vehicles (EVs). The temperature controlling system for the EV battery becomes much simpler, and the closest packing of cells can be realized because the upper-limit temperature of the battery is improved by 40–50 K compared with that in conventional LIBs. In addition, these cells can be used in mid-to-large-sized power storage devices that are operated under hot environments (for example, the tropical and desert regions).

4. Conclusions

Sodium ion batteries consisting of an HC negative electrode, a NaCrO₂ positive electrode, and a Na[FSA]–[C₃C₁pyrr][FSA] ionic liquid have been systematically investigated using coin-type half-cells, coin-type full cells, and large-sized full cells at 273–363 K. First, fundamental charge-discharge characteristics of NaCrO₂ and HC electrodes were presented using coin-type half-cells at 333 and 363 K. Second, a coin-type 1.5 mAh HC/NaCrO₂ full cell was successfully fabricated, giving a specific capacity of 102 mAh (g–NaCrO₂)^{–1} and 252 mAh (g–HC)^{–1} at an operation voltage range of 1.5–3.35 V. Charge-discharge energy efficiencies were as high as 96.9% at 333 K, and 97.5% at 363 K. The cell also exhibited a wide operational temperature range of 283–363 K, and excellent cycle performance of 90% capacity retention after 1000 cycles at 363 K. Finally, a 27 Ah HC/NaCrO₂ full cell was constructed using a mass production process. The calculated volumetric and gravimetric energy densities were 125 Wh L^{–1} and 75 Wh kg^{–1}, respectively. The energy efficiencies were 93.9% at 298 K, and 96.8% at 333 K, as high as those of the coin-type 1.5 mAh full cell. The 27 Ah full cell also showed a wide operational temperature range and a long cycle life of 87% capacity retention after 500 cycles. The performance of the 27 Ah cell was comparable with that of the 1.5 mAh coin-type cell, demonstrating for the first time the successful fabrication of a large-scale sodium-ion battery using a Na[FSA]–[C₃C₁pyrr][FSA] ionic liquid.

Acknowledgements

This study was partly supported by Advanced Low Carbon Technology Research and Development Program (ALCA) of Japan Science and Technology Agency (JST) and the Japanese Ministry of Education Culture, Sports, Science and Technology (MEXT) program “Elements Strategy Initiative to Form Core Research Center” (since 2012).

References

1. J. Tollefson, (2008) Car industry: Charging up the future. *Nature* 456:436-440
2. E. Marris (2008) Energy: Upgrading the grid. *Nature* 454:570-573
3. M. Winter, R.J. Brodd (2004) What Are Batteries, Fuel Cells, and Supercapacitors? *Chem Rev* 104:4245-4269
4. G.L. Soloveichik (2011) Battery technologies for large-scale stationary energy storage. *Annu Rev Chem Biomol Eng* 2:503-527
5. N. Yabuuchi, M. Kajiyama, J. Iwatate, H. Nishikawa, S. Hitomi, R. Okuyama, R. Usui, Y. Yamada, S. Komaba (2012) P2-type $\text{Na}_x[\text{Fe}_{1/2}\text{Mn}_{1/2}]\text{O}_2$ made from earth-abundant elements for rechargeable Na batteries. *Nat Mater* 11:512-517
6. S. Komaba, C. Takei, T. Nakayama, A. Ogata, N. Yabuuchi (2012) Electrochemical intercalation activity of layered NaCrO_2 vs. LiCrO_2 . *Electrochem Commun* 12:355-358
7. S. Komaba, N. Yabuuchi, T. Nakayama, A. Ogata, T. Ishikawa, I. Nakai (2012) Study on the Reversible Electrode Reaction of $\text{Na}_{1-x}\text{Ni}_{0.5}\text{Mn}_{0.5}\text{O}_2$ for a Rechargeable Sodium-Ion Battery. *Inorg Chem* 51:6211-6220
8. J. Billaud, G. Singh, A.R. Armstrong, E. Gonzalo, V. Roddatis, M. Armand, T. Rojjob, P.G. Bruce (2014) $\text{Na}_{0.67}\text{Mn}_{1-x}\text{Mg}_x\text{O}_2$ ($0 \leq x \leq 0.2$): a high capacity cathode for sodium-ion batteries. *Energy Environ Sci* 7:1387-1391
9. J.J. Ding, Y.N. Zhou, Q. Sun, Z.W. Fu (2012) Cycle performance improvement of NaCrO_2 cathode by carbon coating for sodium ion batteries. *Electrochem Commun* 22:85-88
10. N. Yabuuchi, H. Yoshida, S. Komaba (2012) Crystal Structures and Electrode Performance of $\alpha\text{-NaFeO}_2$ for Rechargeable Sodium Batteries. *Electrochemistry* 80:716-719
11. P. Vassilaras, X.H. Ma, X. Li, G. Ceder (2013) Electrochemical Properties of Monoclinic NaNiO_2 . *J Electrochem Soc* 160:A207-A211
12. M. Sathiya, K. Hemalatha, K. Ramesha, J.M. Tarascon, A.S. Prakash (2012) Synthesis, Structure, and Electrochemical Properties of the Layered Sodium Insertion Cathode Material: $\text{NaNi}_{1/3}\text{Mn}_{1/3}\text{Co}_{1/3}\text{O}_2$. *Chem Mater* 24:1846-1853
13. H. Yoshida, N. Yabuuchi, S. Komaba (2013) $\text{NaFe}_{0.5}\text{Co}_{0.5}\text{O}_2$ as high energy and power positive electrode for Na-ion batteries. *Electrochem Commun* 34:60-63

14. B.M. de Boisse, D. Carlier, M. Guignard, C. Delmas (2013) Structural and Electrochemical Characterizations of P2 and New O3-Na_xMn_{1-y}Fe_yO₂ Phases Prepared by Auto-Combustion Synthesis for Na-Ion Batteries. *J Electrochem Soc* 160:A569-A574
15. J. Zhao, J. Xu, D.H. Lee, N. Dimov, Y.S. Meng, S. Okada (2014) Electrochemical and thermal properties of P2-type Na_{2/3}Fe_{1/3}Mn_{2/3}O₂ for Na-ion batteries. *J Power Sources* 264:235-239
16. J.M. Tarascon (2010) Is lithium the new gold? *Nat Chem* 2:510
17. W. Tahil (2007) The Trouble With Lithium. <http://go.nature.com/jhDqLH>. Accessed 1 September 2015
18. W. Tahil (2008) The Trouble With Lithium 2. <http://go.nature.com/AWITRo>. Accessed 1 September 2015
19. Y.F.Y. Yao, J.T. Kummer (1967) Ion exchange properties of and rates of ionic diffusion in beta-alumina. *J Inorg Nucl Chem* 29:2453-2475
20. J.L. Sudworth (1984) The sodium/sulphur battery. *J Power Sources* 11:143-154
21. J. Coetzer (1986) A new high energy density battery system. *J Power Sources* 18:377-380
22. C.H. Dustmann (2004) Advances in ZEBRA batteries. *J Power Sources* 127:85-92
23. K.B. Hueso, M. Armand, T. Rojo (2010) High temperature sodium batteries: status, challenges and future trends. *Energy Environ Sci* 6:734-749
24. X.C. Lu, G.G. Xia, J.P. Lemmon, Z.G. Yang (2010) Advanced materials for sodium-beta alumina batteries: Status, challenges and perspectives. *J Power Sources* 195:2431-2442
25. K. Kubota, N. Yabuuchi, H. Yoshida, M. Dahbi, S. Komaba (2014) Layered oxides as positive electrode materials for Na-ion batteries. *MRS Bulletin* 39:416-422
26. H. Pan, Y. S. Hu, L. Chen (2013) Room-temperature stationary sodium-ion batteries for large-scale electric energy storage. *Energy Environ Sci* 6:2338-2360
27. N. Yabuuchi, K. Kubota, M. Dahbi, S. Komaba (2014) Research Development on Sodium-Ion Batteries. *Chem Rev* 114:11636-11682
28. K. Kubota, T. Nohira, T. Goto, R. Hagiwara (2008) Novel inorganic ionic liquids possessing low melting temperatures and wide electrochemical windows: Binary mixtures of alkali bis(fluorosulfonyl)amides. *Electrochem Commun* 10:1886-1888
29. K. Kubota, T. Nohira, R. Hagiwara (2010) Thermal Properties of Alkali Bis(fluorosulfonyl)amides

- and Their Binary Mixtures. *J Chem Eng Data* 55:3142-3146
30. K. Kubota, T. Nohira, R. Hagiwara (2012) New inorganic ionic liquids possessing low melting temperatures and wide electrochemical windows: Ternary mixtures of alkali bis(fluorosulfonyl)amides. *Electrochim Acta* 66:320-324
 31. R. Hagiwara, K. Tamaki, K. Kubota, T. Goto, T. Nohira (2008) Thermal properties of mixed alkali bis(trifluoromethylsulfonyl)amides. *J Chem Eng Data* 53:355-358
 32. T. Nohira, T. Ishibashi, R. Hagiwara (2012) Properties of an intermediate temperature ionic liquid NaTFSA–CsTFSA and charge–discharge properties of NaCrO₂ positive electrode at 423 K for a sodium secondary battery. *J Power Sources* 205:506-509
 33. A. Fukunaga, T. Nohira, Y. Kozawa, R. Hagiwara, S. Sakai, K. Nitta, S. Inazawa (2012) Intermediate–temperature ionic liquid NaFSA–KFSA and its application to sodium secondary batteries. *J Power Sources* 209:52-56
 34. C.S. Ding, T. Nohira, K. Kuroda, R. Hagiwara, A. Fukunaga, S. Sakai, K. Nitta, S. Inazawa (2013) NaFSA–C₁C₃pyrFSA ionic liquids for sodium secondary battery operating over a wide temperature range. *J Power Sources* 238:296-300
 35. X. Xia, J.R. Dahn (2012) NaCrO₂ is a Fundamentally Safe Positive Electrode Material for Sodium–Ion Batteries with Liquid Electrolytes. *Electrochem Solid–State Lett* 15:A1-A4
 36. M. Dahbi, T. Nakano, N. Yabuuchi, T. Ishikawa, K. Kubota, M. Fukunishi, S. Shibahara, J.Y. Son, Y.T. Cui, H. Oji, S. Komaba (2014) Sodium carboxymethyl cellulose as a potential binder for hard–carbon negative electrodes in sodium–ion batteries. *Electrochem Comm* 44:66-69
 37. K. Gotoh, T. Ishikawa, S. Shimadzu, N. Yabuuchi, S. Komaba, K. Takeda, A. Goto, K. Deguchi, S. Ohki, K. Hashi, T. Shimizu, H. Ishida (2013) NMR study for electrochemically inserted Na in hard carbon electrode of sodium ion battery. *J Power Sources* 225:137-140
 38. S. Komaba, W. Murata, T. Ishikawa, N. Yabuuchi, T. Ozeki, T. Nakayama, A. Ogata, K. Gotoh, K. Fujiwara (2011) Electrochemical Na insertion and solid electrolyte interphase for hard–carbon electrodes and application to Na–ion batteries. *Adv Funct Mater* 21:3859-3867
 39. A. Fukunaga, T. Nohira, R. Hagiwara, K. Numata, E. Itani, S. Sakai, K. Nitta, S. Inazawa (2014) A safe and high–rate negative electrode for sodium–ion batteries: Hard carbon in NaFSA–C₁C₃pyrFSA ionic liquid at 363 K. *J Power Sources* 246:387-391

40. C.J. Rydh, B.A. Sandén (2005) Energy analysis of batteries in photovoltaic systems. Part II: Energy return factors and overall battery efficiencies. *Energ Convers Manag* 46:1980-2000
41. H. Chen, T.N. Cong, W. Yang, C. Tan, Y. Li, Y. Ding (2009) Progress in electrical energy storage system: A critical review. *Prog Nat Sci* 19:291-312
42. T. Iguchi, K. Okamoto, J. Kuratomi, K. Ohkawa, K. Kohno, S. Izuchi (2004) Development of Lithium-Ion Battery “EX25A” with New Positive Active Material of $\text{LiCo}_x\text{Mn}_y\text{Ni}_z\text{O}_2$ ($x+y+z=1$): GS Yuasa Technical Report 1:25-31
43. C.Y. Chen, K. Matsumoto, T. Nohira, R. Hagiwara, A. Fukunaga, S. Sakai, K. Nitta, S. Inazawa (2013) Electrochemical and structural investigation of NaCrO_2 as a positive electrode for sodium secondary battery using inorganic ionic liquid NaFSA–KFSA: *J Power Sources* 237:52-57
44. C. Delmas, C. Fouassier, P. Hagenmuller (1980) Structural classification and properties of layered oxides: *Physica B+C* 99:81-85

Tables

Table 1 Charge and discharge conditions for Na/NaCrO₂, Na/HC, and HC/NaCrO₂ cells.

Cell	Charge rate	Discharge rate	Cut-off voltages
Na/NaCrO ₂	20 mA (g-NaCrO ₂) ⁻¹	20–600 mA (g-NaCrO ₂) ⁻¹	2.5 and 3.5 V
Na/HC	25 mA (g-HC) ⁻¹	25–1000 mA (g-HC) ⁻¹	0.005 and 1.2 V
HC/NaCrO ₂	20–100 mA (g-NaCrO ₂) ⁻¹	10–600 mA (g-NaCrO ₂) ⁻¹	1.5 and 3.35 V

Table 2 Coulombic and energy efficiencies for a 1.5 mAh HC/Na[FSA]-[C₃C₁pyrr][FSA]/NaCrO₂

full cell. Operating temperatures: 298, 333, and 363 K. Charge–discharge rate: 0.3 mA.

Operating temperature	Coulombic efficiency	Energy efficiency
363 K	99.85%	97.5%
333 K	99.84%	96.9%
298 K	99.78%	93.2%

Figure captions

Figure 1 XRD pattern of obtained NaCrO_2 powder.

Figure 2 Appearance of a 27 Ah $\text{HC}/\text{Na}[\text{FSA}]-[\text{C}_3\text{C}_1\text{pyrr}][\text{FSA}]/\text{NaCrO}_2$ prismatic cell. External size: $113 \times 150 \times 38$ mm. Weight: 1.08 kg.

Figure 3 (a) A charge–discharge curve for a $\text{Na}/\text{Na}[\text{FSA}]-[\text{C}_3\text{C}_1\text{pyrr}][\text{FSA}]/\text{NaCrO}_2$ cell at 363 K. Charge–discharge rate: $20 \text{ mA (g-NaCrO}_2\text{)}^{-1}$. (b) Discharge curves at 363 K and (c) discharge curves at 333 K. Charge rate: $20 \text{ mA (g-NaCrO}_2\text{)}^{-1}$. Discharge rate: $10\text{--}600 \text{ mA (g-NaCrO}_2\text{)}^{-1}$. Cut-off voltages: 2.5 V and 3.5 V.

Figure 4 Rate dependence of discharge capacity for a $\text{Na}/\text{Na}[\text{FSA}]-[\text{C}_3\text{C}_1\text{pyrr}][\text{FSA}]/\text{NaCrO}_2$ cell. Charge rate: $20 \text{ mA (g-NaCrO}_2\text{)}^{-1}$, discharge rate: $10\text{--}600 \text{ mA (g-NaCrO}_2\text{)}^{-1}$. Operation temperature: 333 and 363 K.

Figure 5 (a) A charge–discharge curve for a $\text{Na}/\text{Na}[\text{FSA}]-[\text{C}_3\text{C}_1\text{pyrr}][\text{FSA}]/\text{HC}$ cell at 363 K. Charge–discharge rate: $50 \text{ mA (g-HC)}^{-1}$. (b) Discharge curves at 363 K and (c) discharge curves at 333 K. Charge rate: $50 \text{ mA (g-HC)}^{-1}$. Discharge rate: $25\text{--}1000 \text{ mA (g-HC)}^{-1}$. Cut-off voltages: 0.005 V and 1.2 V.

Figure 6 Rate dependence of discharge capacity for a $\text{Na}/\text{Na}[\text{FSA}]-[\text{C}_3\text{C}_1\text{pyrr}][\text{FSA}]/\text{HC}$ cell. Charge rate: $50 \text{ mA (g-HC)}^{-1}$, discharge rate: $25\text{--}1000 \text{ mA (g-HC)}^{-1}$. Operation temperature: 363 and 333 K.

Figure 7 (a) A charge–discharge curve for a 1.5 mAh $\text{HC}/\text{Na}[\text{FSA}]-[\text{C}_3\text{C}_1\text{pyrr}][\text{FSA}]/\text{NaCrO}_2$ full cell at 363 K. Charge–discharge rate: 0.3 mA. (b) Discharge curves at 363 K, and (c) discharge curves at 333 K. Charge rate: 0.3 mA. Discharge rate: $0.3\text{--}9.0 \text{ mA}$. Cut-off voltages: 1.5 V and 3.4 V.

Figure 8 Discharge curves for a 1.5 mAh $\text{HC}/\text{Na}[\text{FSA}]-[\text{C}_3\text{C}_1\text{pyrr}][\text{FSA}]/\text{NaCrO}_2$ full cell at 298 and 283 K. Charge condition: 0.3 mA CC–CV (to 0.075 mA) at 298 K. Discharge rate: 0.3 mA (298 K) and 0.15 mA (283 K). Cut-off voltages: 1.5 V and 3.35 V.

Figure 9 Rate dependence of the discharge capacity for a 1.5 mAh $\text{HC}/\text{Na}[\text{FSA}]-[\text{C}_3\text{C}_1\text{pyrr}][\text{FSA}]/\text{NaCrO}_2$ full cell. Charge condition: 0.3 mA CC (313–363 K) and 0.3 mA CC–CV (to 0.075 mA) at 298 K (273–298 K). Discharge rate: $0.15\text{--}9.0 \text{ mA}$. Operation temperature: 273–363 K.

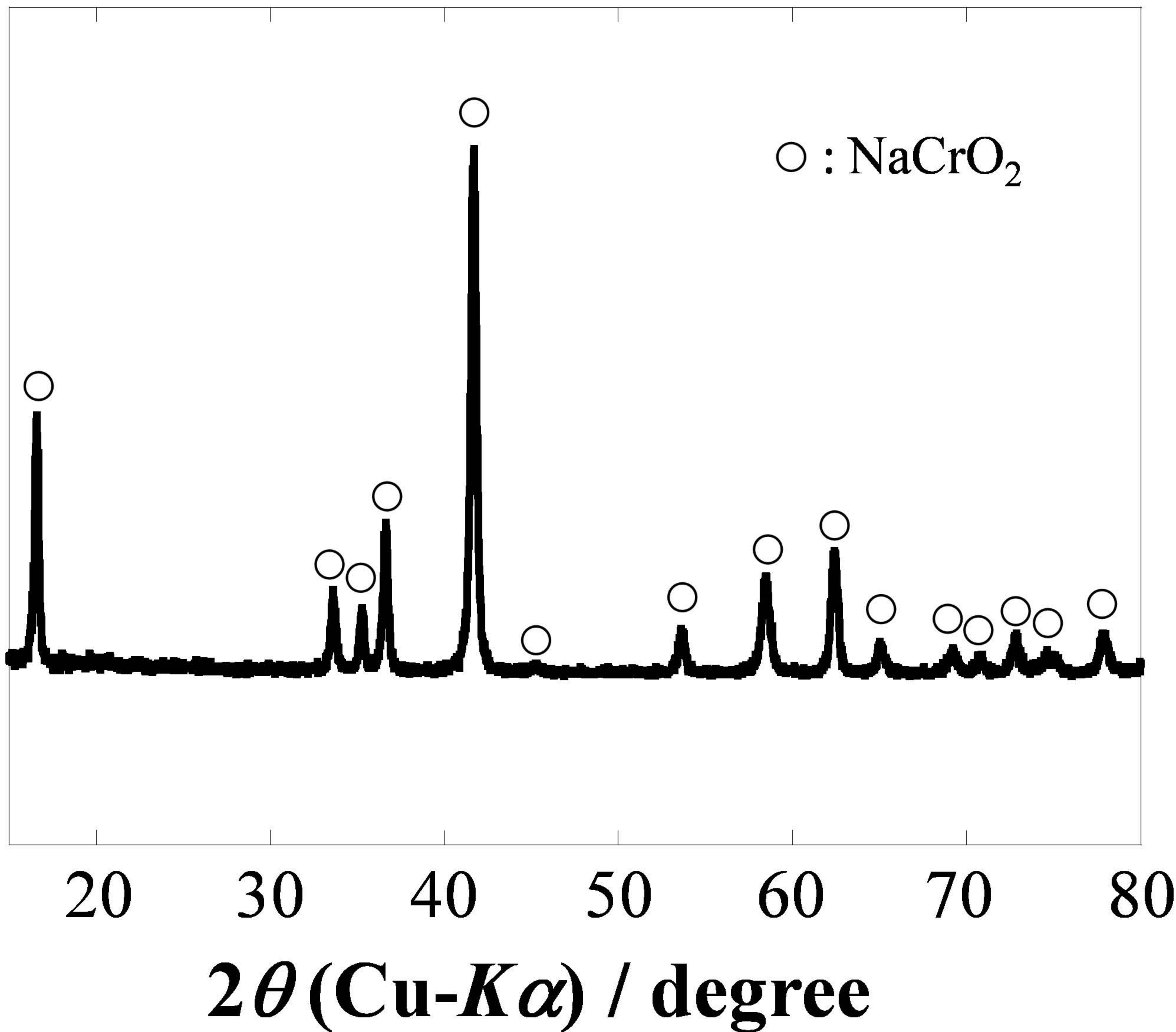
Figure 10 Cycle property for a HC/Na[FSA]–[C₃C₁pyrr][FSA]/NaCrO₂ full cell. Charge–discharge rate: 1.5 mA. Operation temperature: 363 K and 333 K. Cut-off voltages: 1.5 V and 3.35 V.

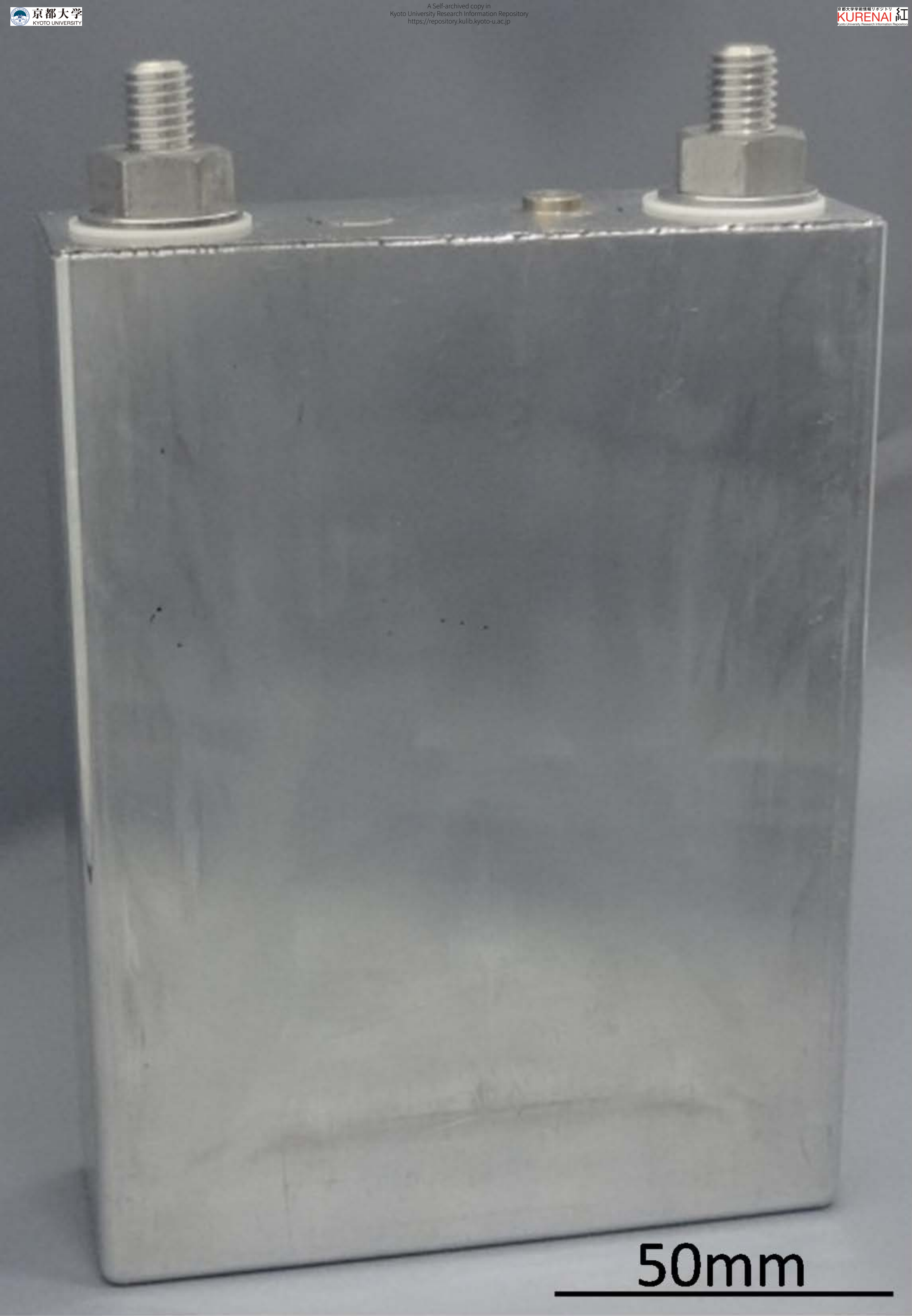
Figure 11 Charge–discharge curves for a 27 Ah HC/Na[FSA]–[C₃C₁pyrr][FSA]/NaCrO₂ full cell at 298 and 333 K. Charge–discharge rate: 2.7 A (298 K) and 10 A (333 K). Cut-off voltages: 1.5 V and 3.35 V.

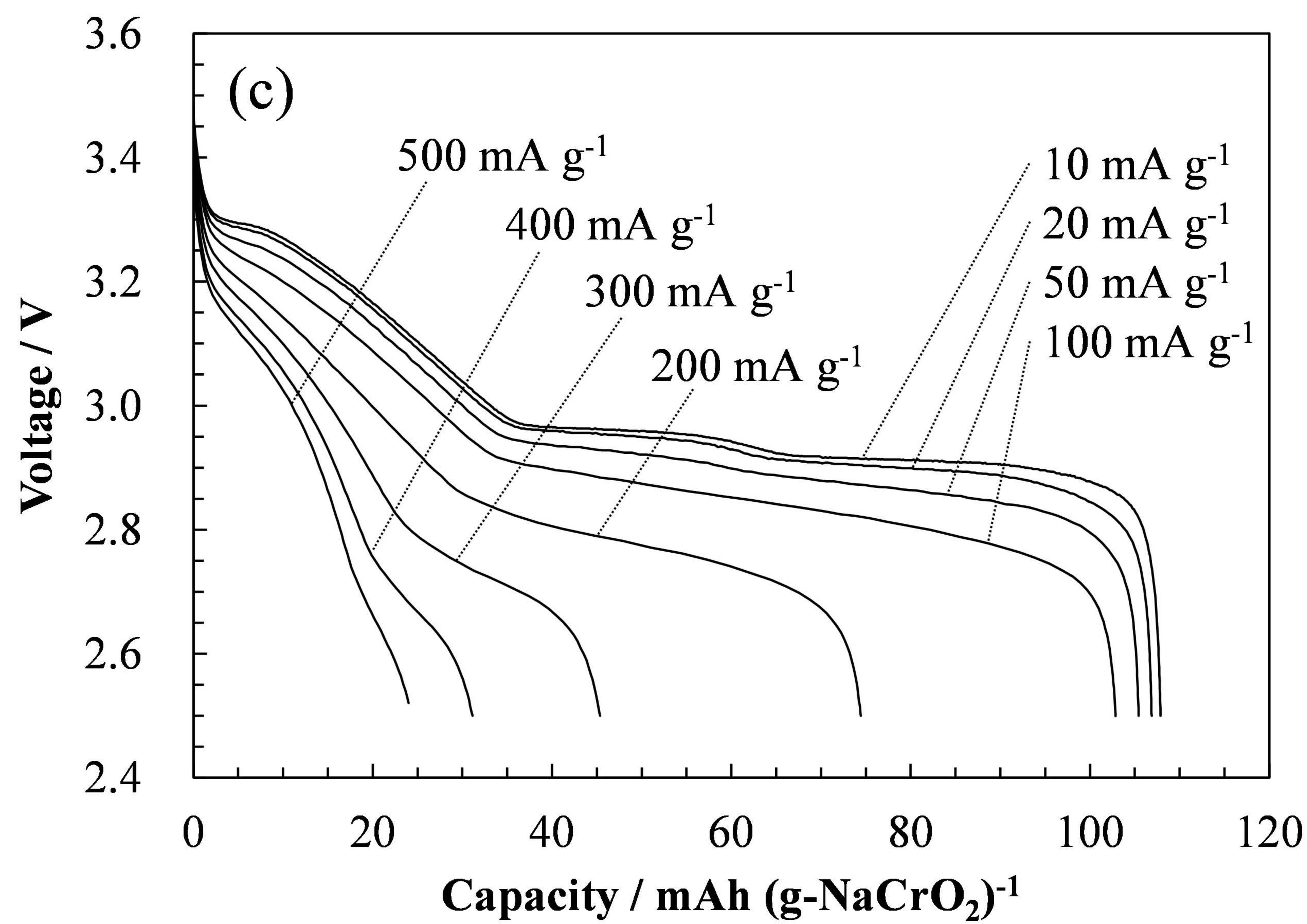
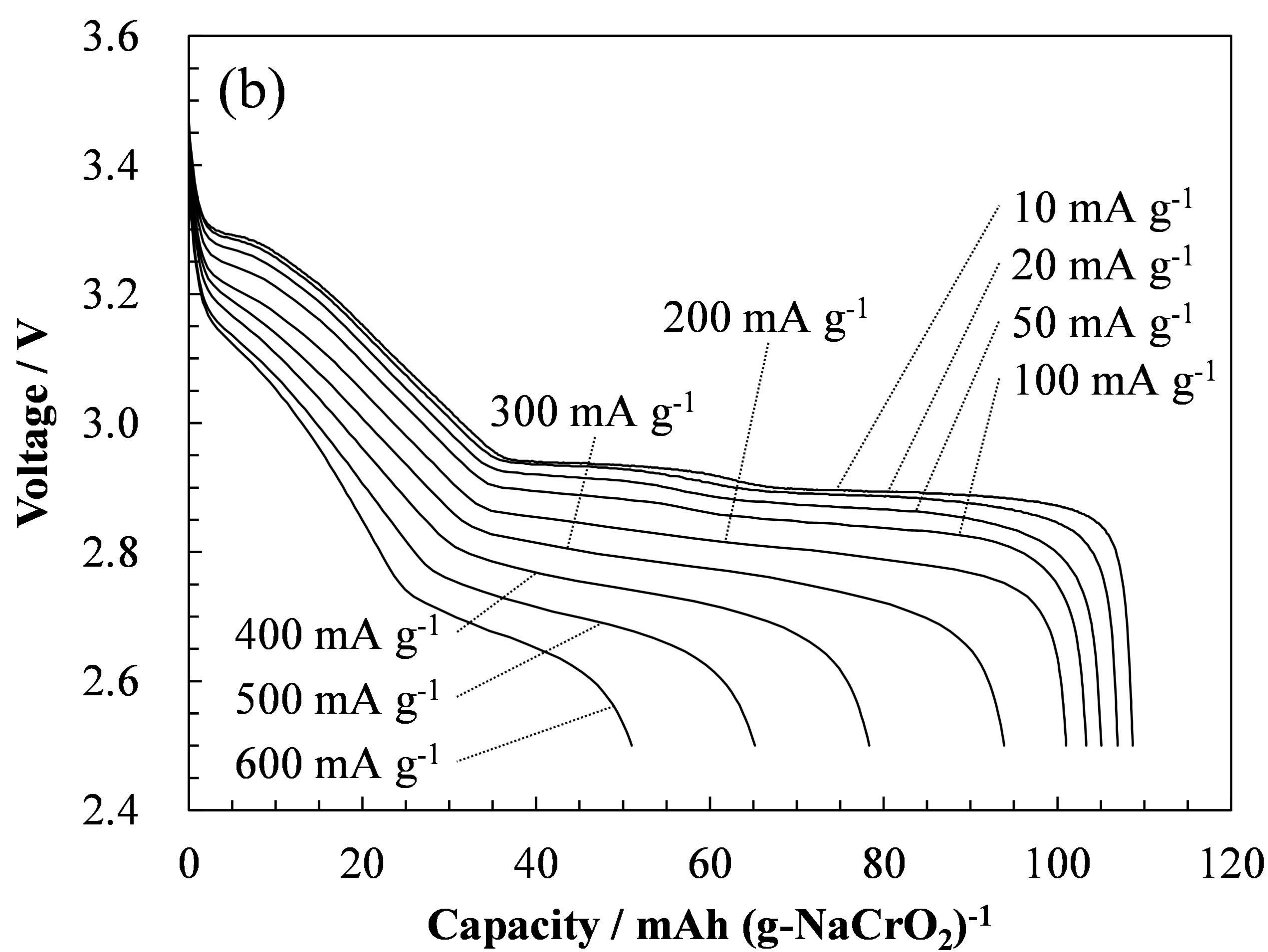
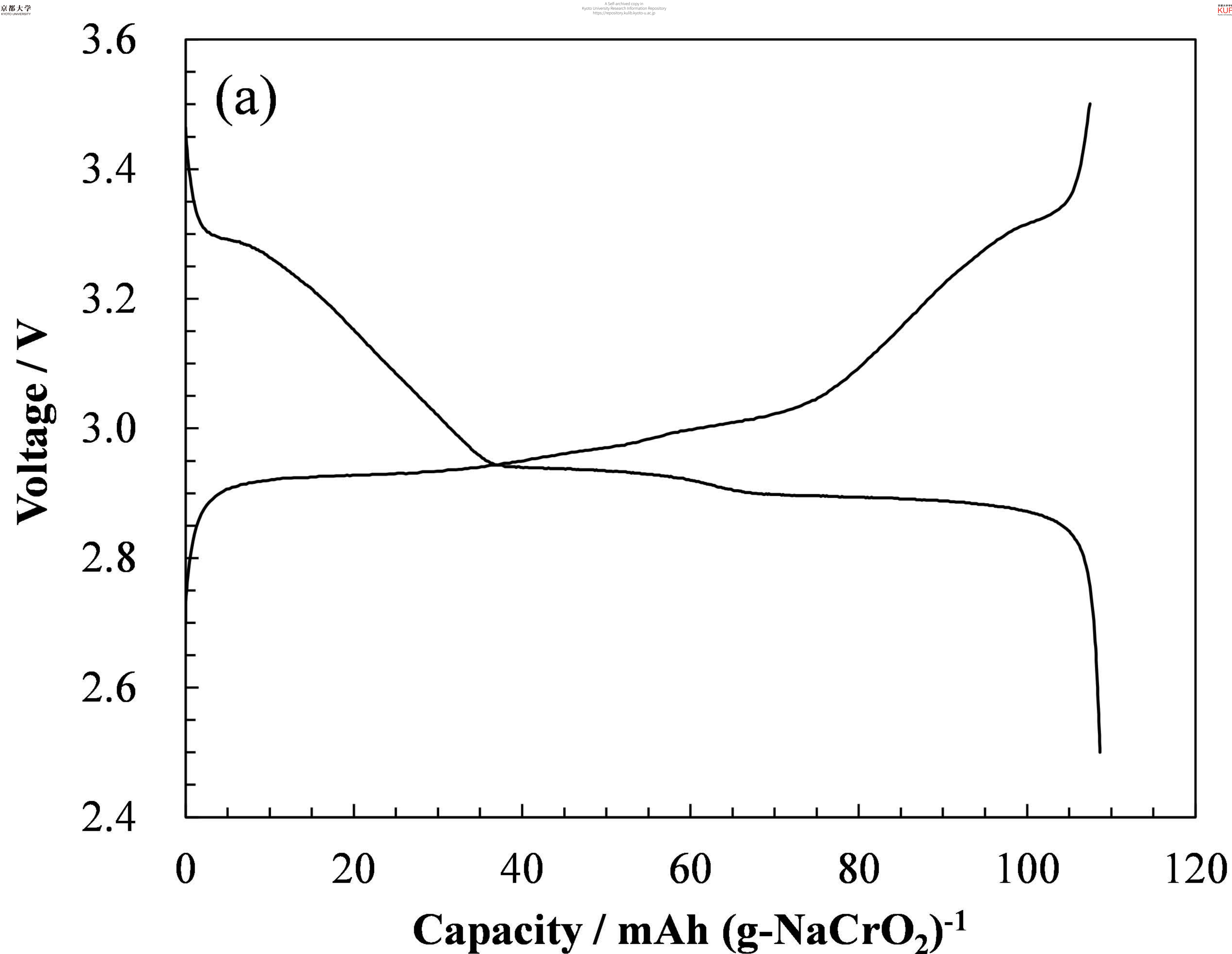
Figure 12 Rate dependence of discharge capacity for a 27 Ah HC/Na[FSA]–[C₃C₁pyrr][FSA]/NaCrO₂ full cell. Charge rate: 2.7 A (283–293 K) and 5.4 A (313–363 K), discharge rate: 2.7–81 A. Operation temperature: 283–363 K.

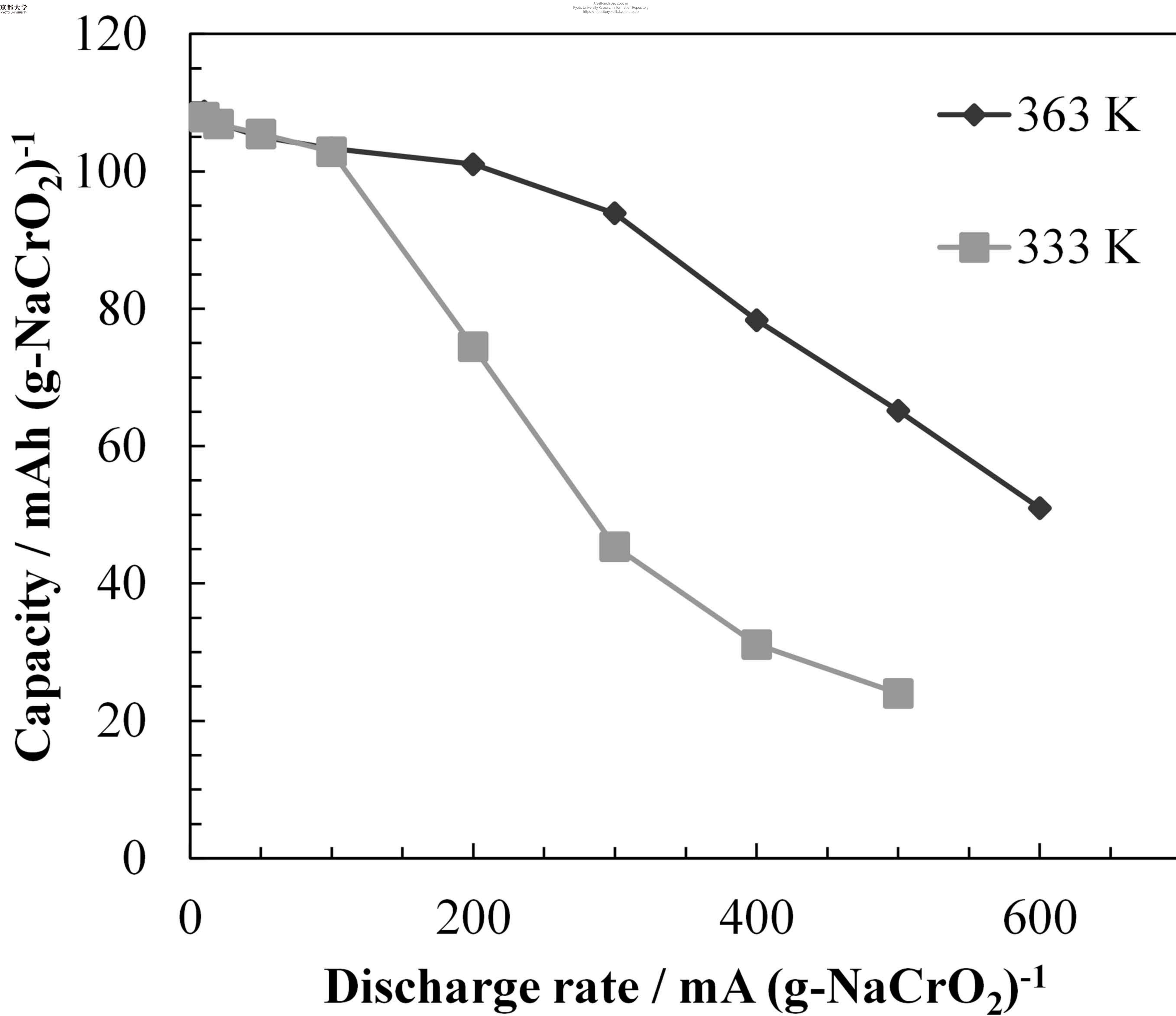
Figure 13 Cycle property for a 27 Ah HC/Na[FSA]–[C₃C₁pyrr][FSA]/NaCrO₂ full cell. Charge–discharge rate: 10 A. Operation temperature: 333 K. Cut-off voltages: 1.5 V and 3.35 V.

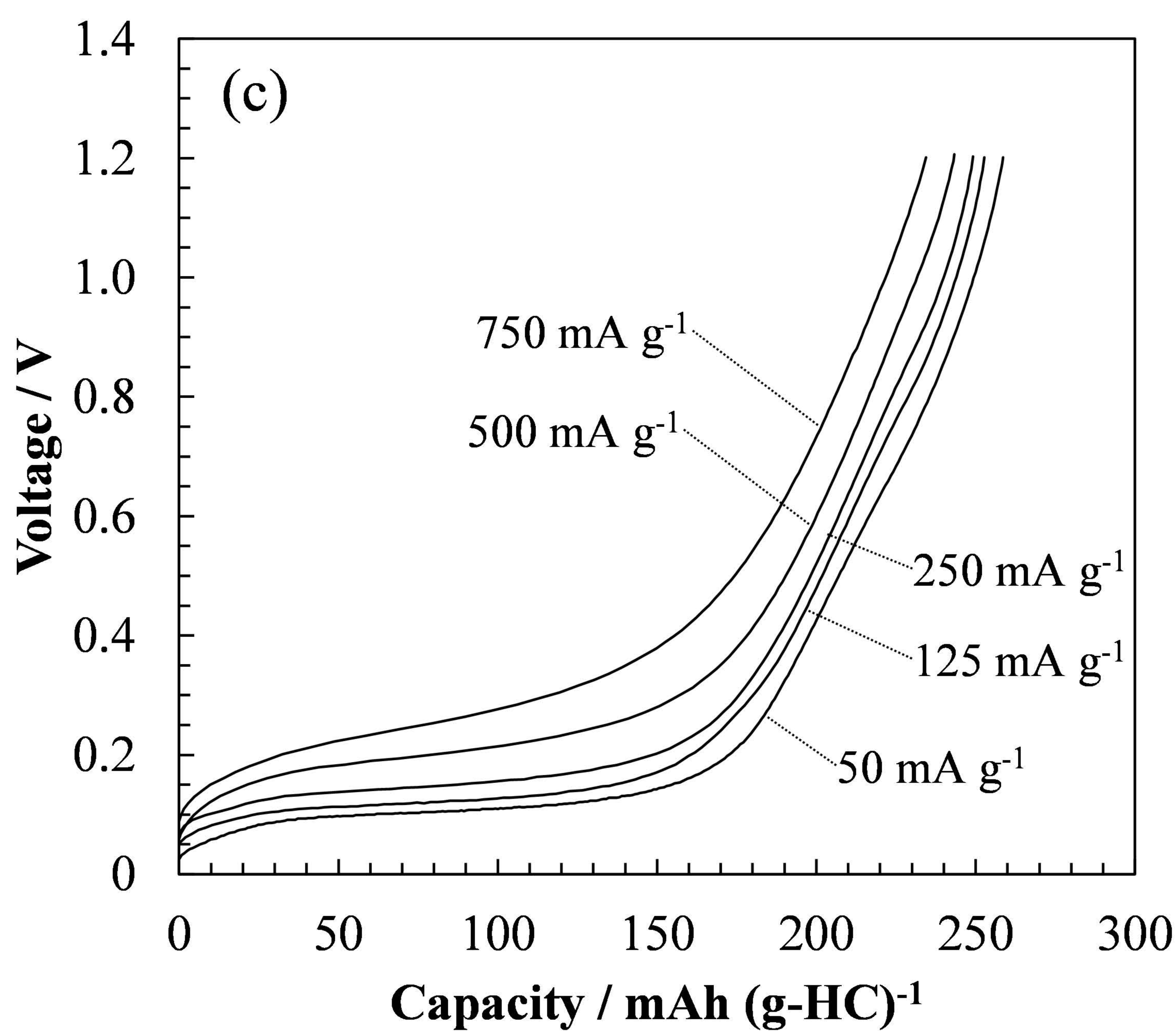
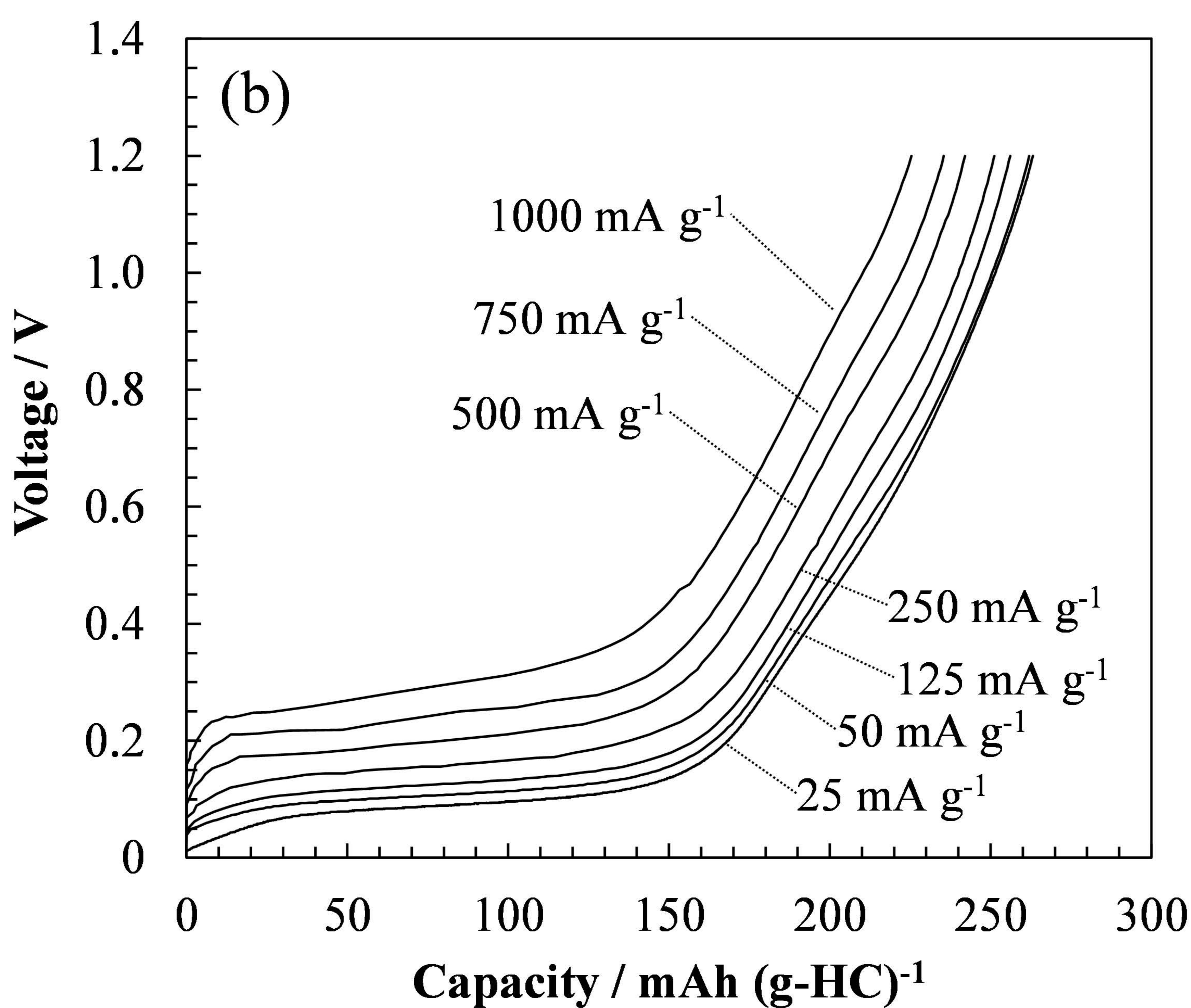
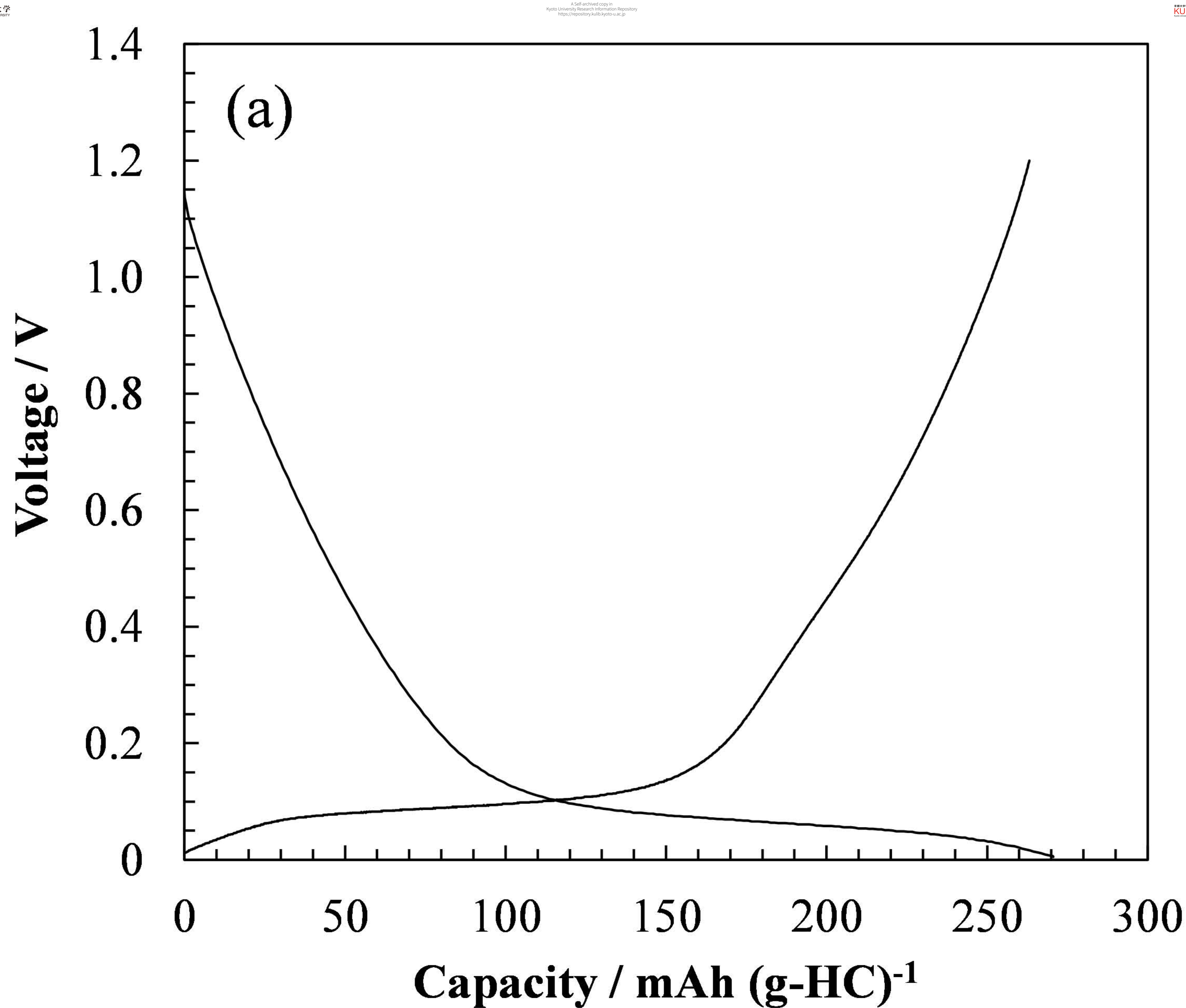
Intensity / a.u.

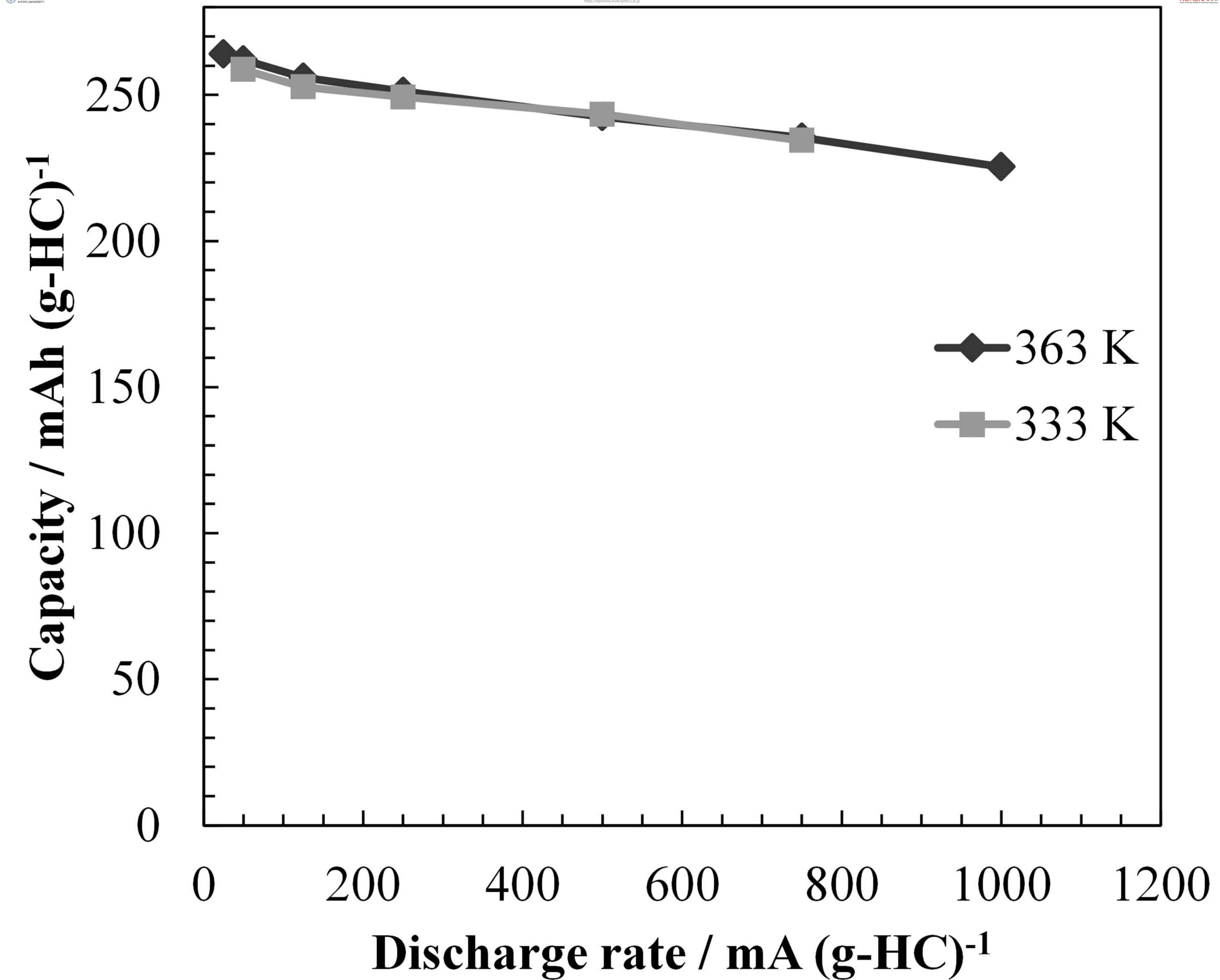


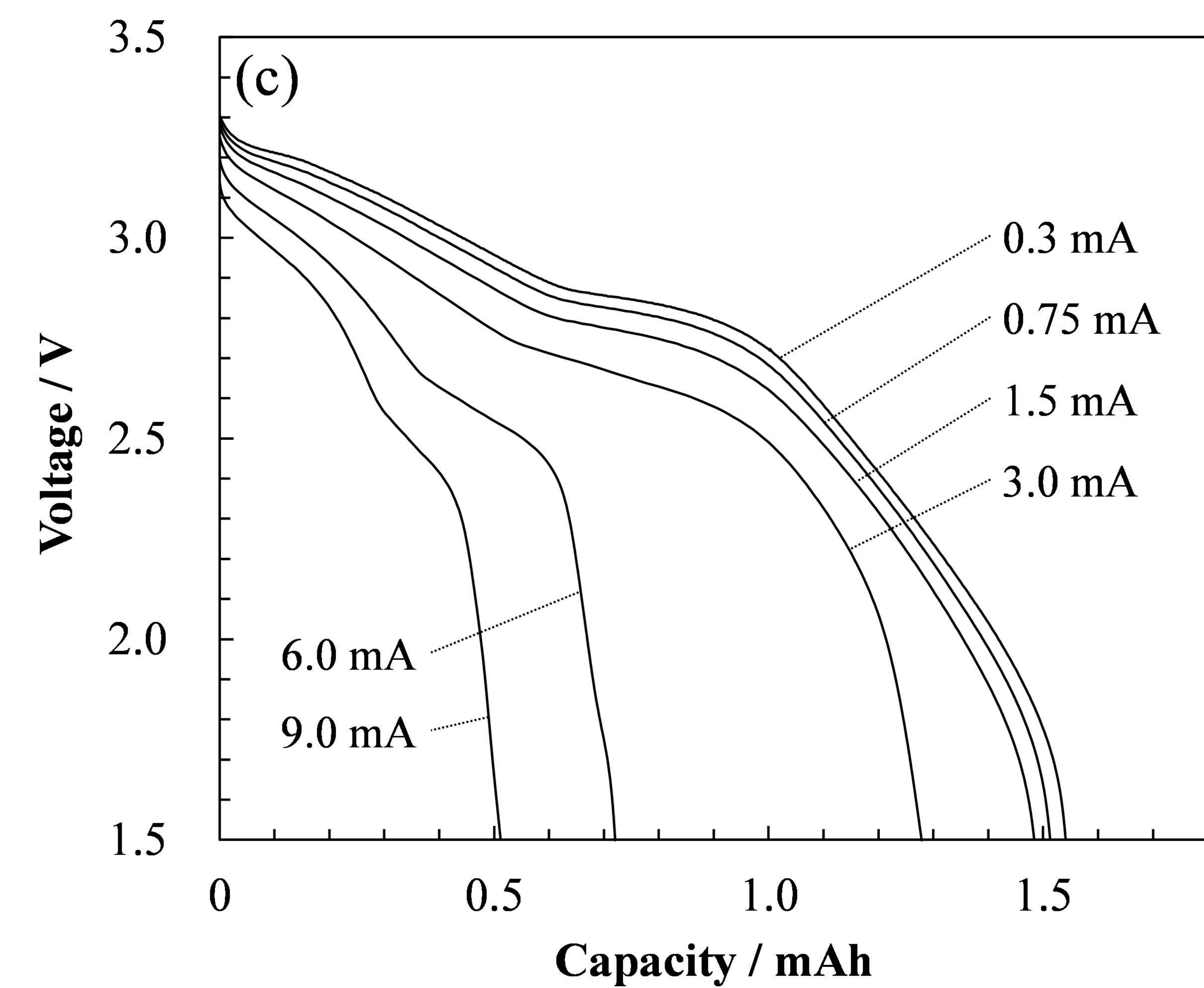
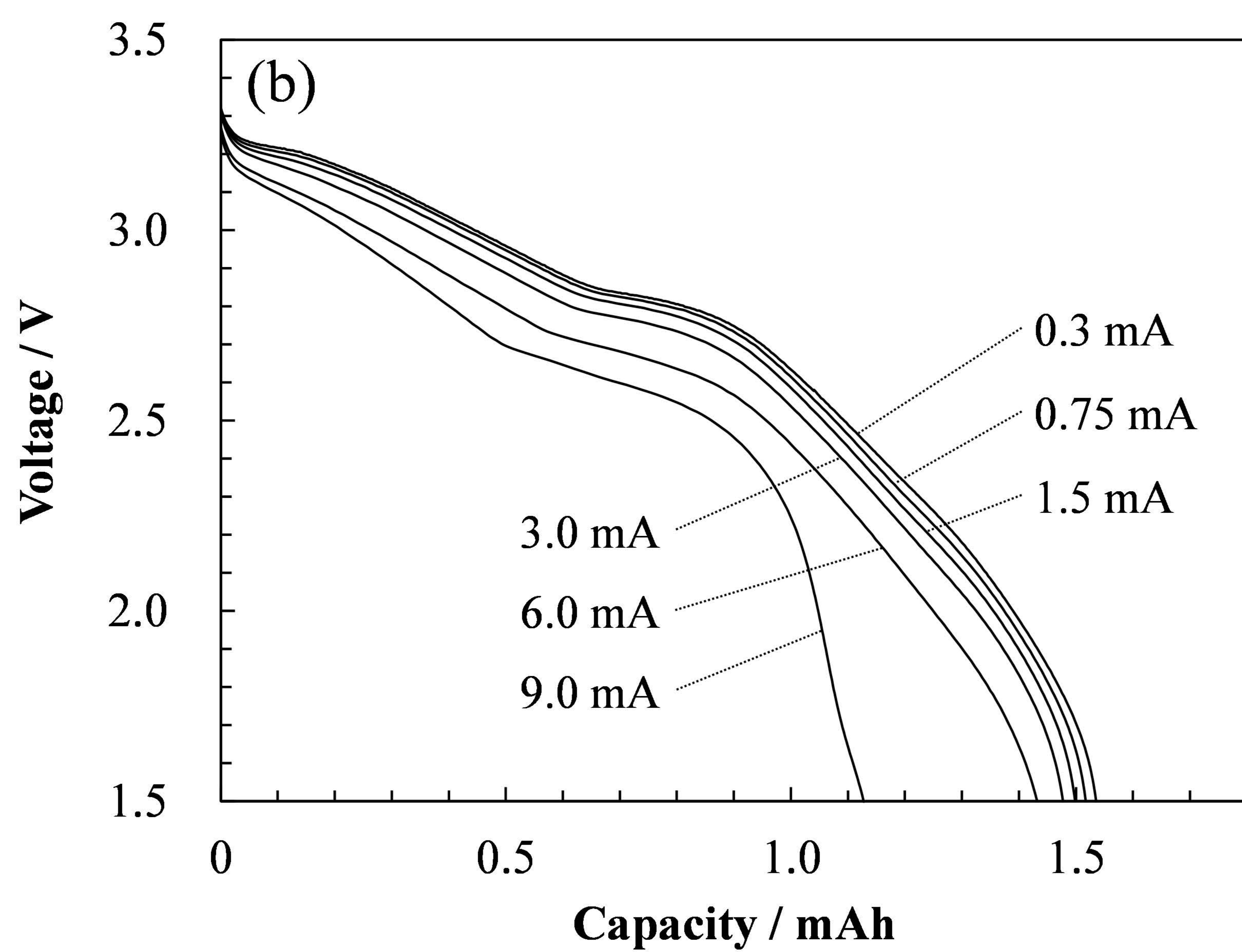
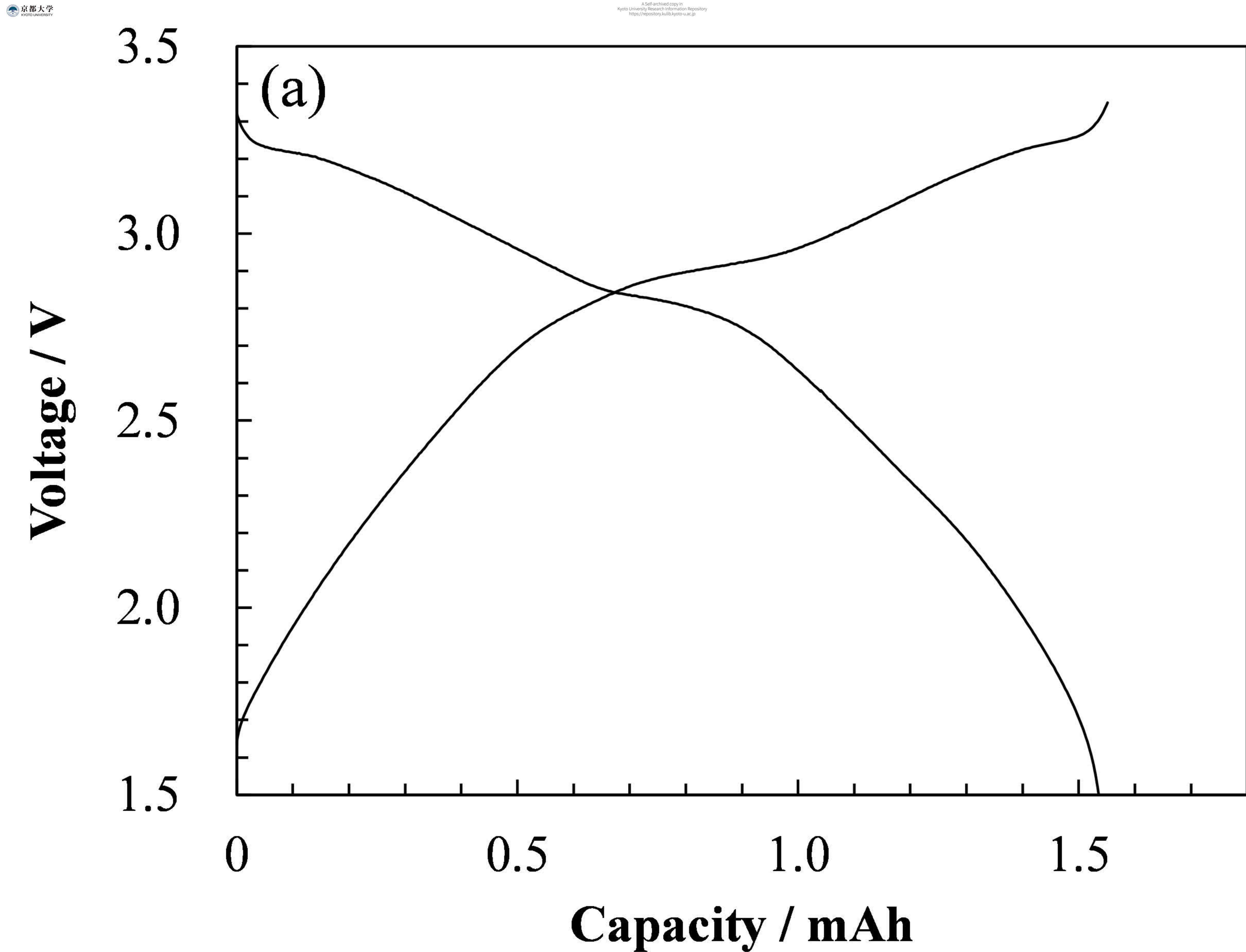


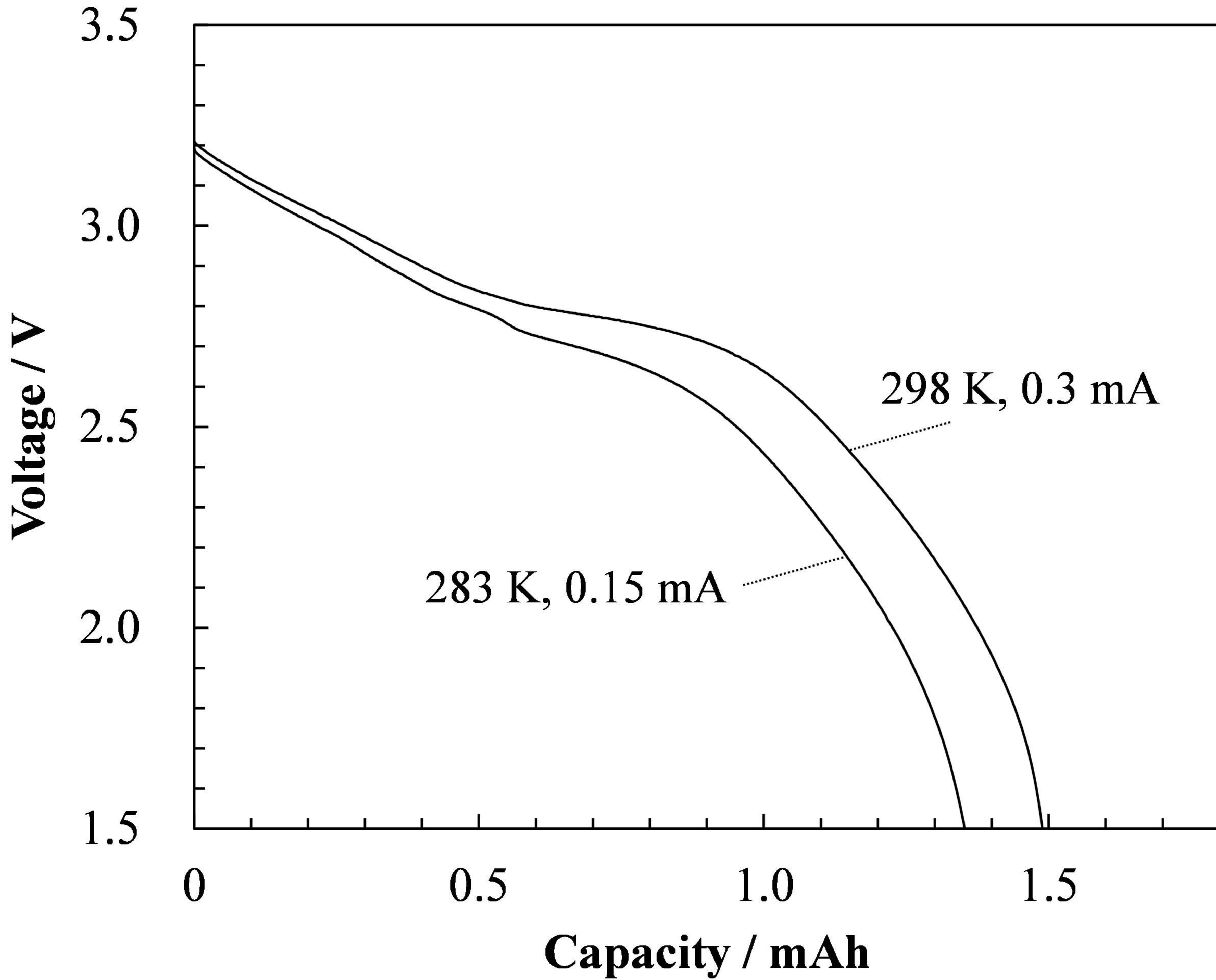












Capacity / mAh

1.5
1
0.5
0

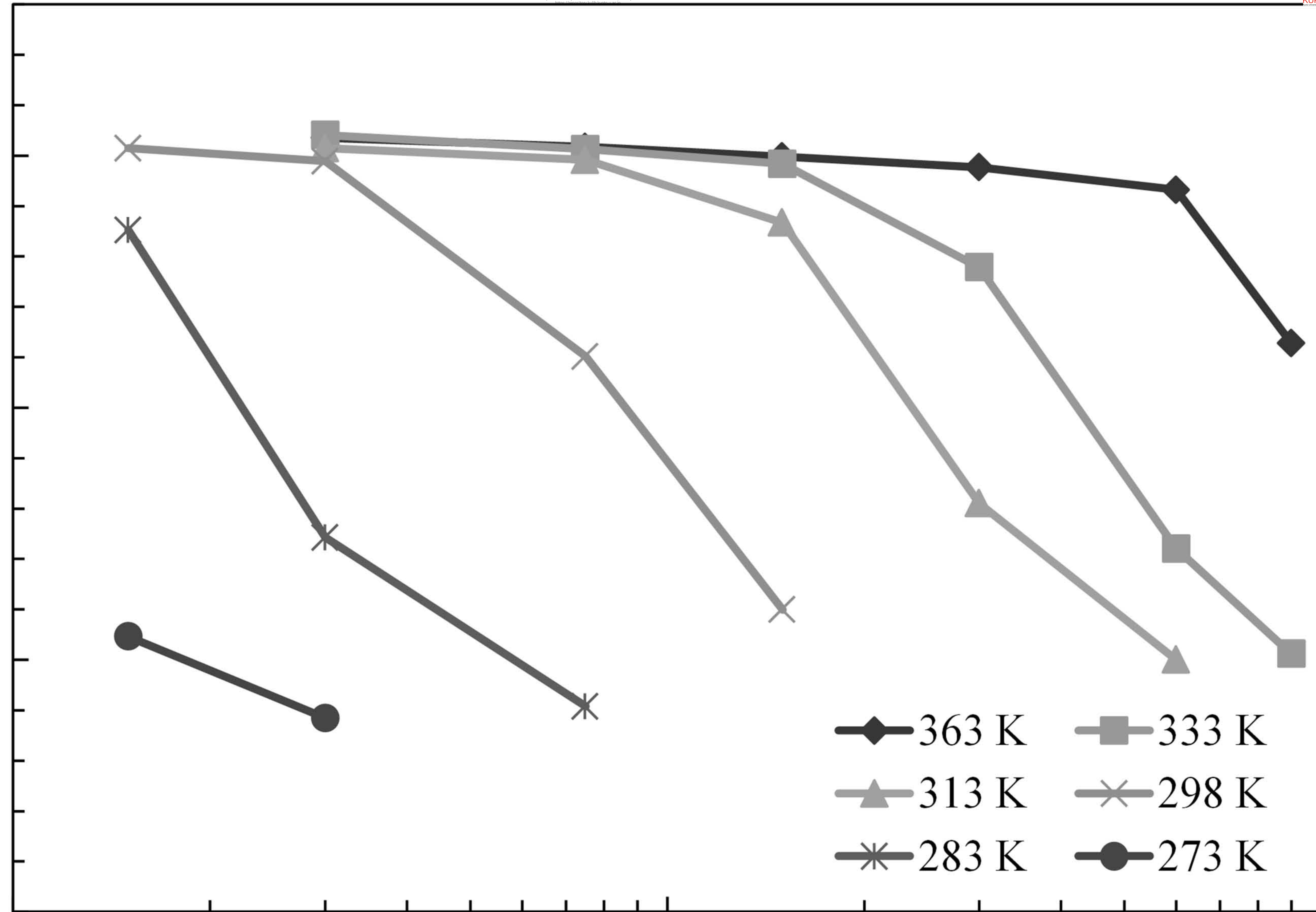
0.1

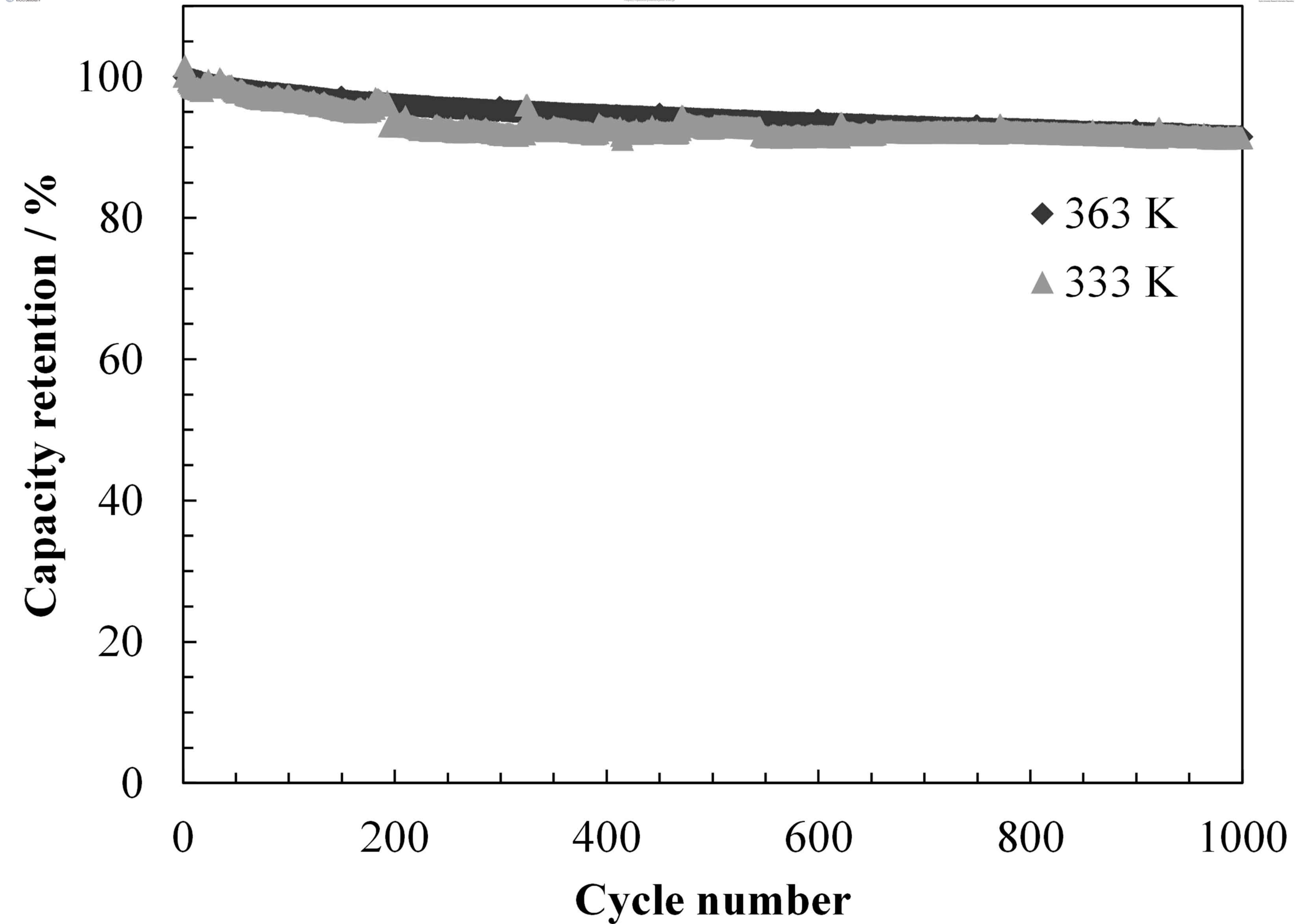
1

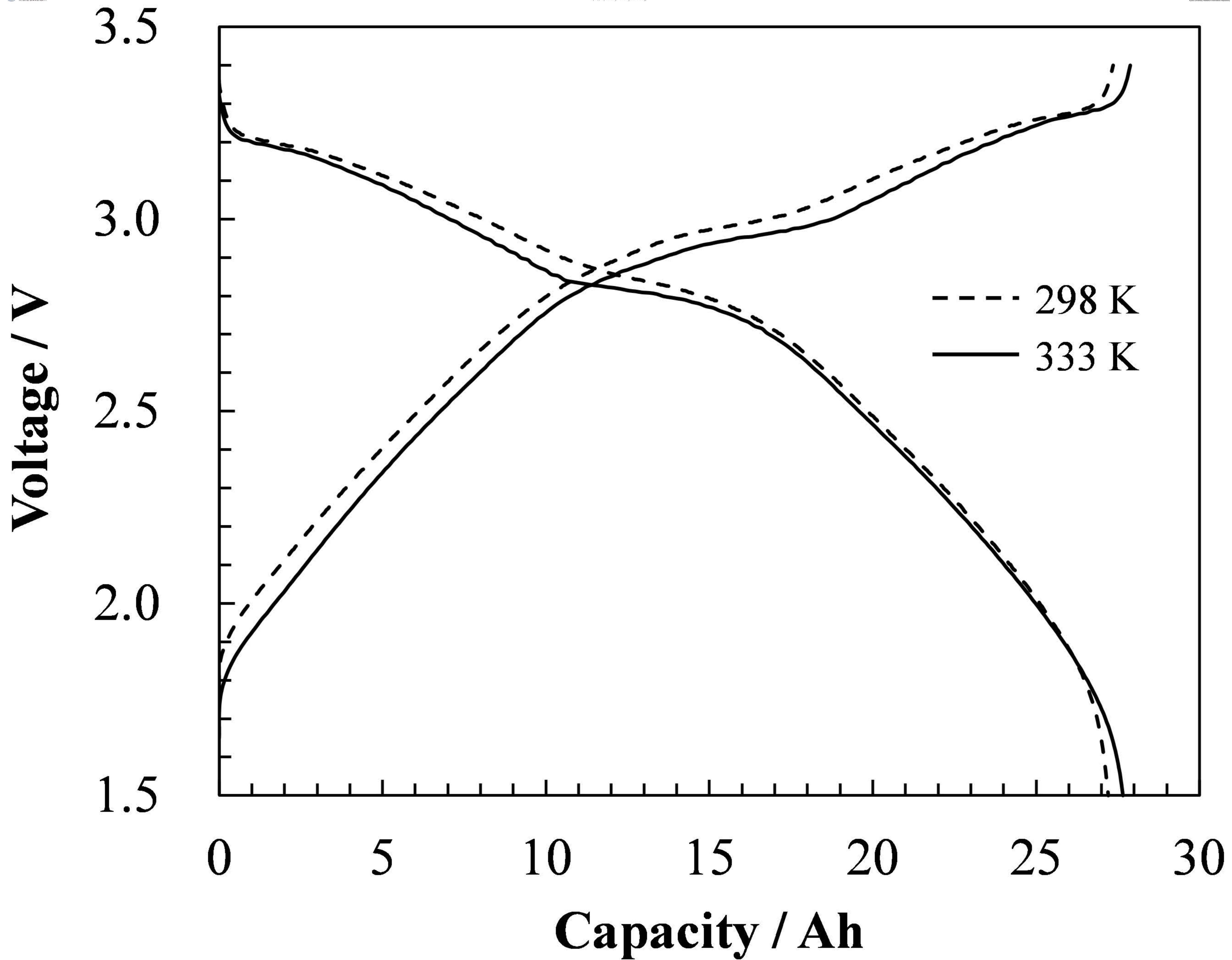
10

Discharge rate / mA

◆ 363 K ■ 333 K
 ▲ 313 K ✕ 298 K
 ✕ 283 K ● 273 K







Capacity / Ah

